

# Synthetic Aperture Radar Image Processing Techniques for Damage Detection of FRP-concrete Systems

Tzuyang Yu

Department of Civil and Environmental Engineering  
University of Massachusetts Lowell  
Lowell, Massachusetts 01854, U.S.A.

## ABSTRACT

Electromagnetic imaging enables researchers and engineers to assess the surface and subsurface condition of concrete structures using radar and microwave sensors. Among existing radar imaging methods, synthetic aperture radar (SAR) imaging offers flexible resolution for various purposes in condition assessment. In this paper, two novel SAR image processing techniques are reported for the subsurface condition assessment of FRP (fiber reinforced polymer)-strengthened concrete systems; mathematical morphology (MM) and the K-R-I transform. Glass FRP (GFRP) and carbon CFRP (CFRP) strengthened concrete cylinders are used as examples. From our experimental results, it is found that both techniques are capable of quantifying SAR images for condition assessment. It is also found that Euler's number and the coefficient of correlation of K-R-I curves of SAR images can be used for monitoring subsurface changes in FRP-concrete systems.

**Keywords:** SAR imaging, dielectrics, concrete, subsurface sensing, damage detection, mathematical morphology, K-R-I transform

## 1. INTRODUCTION

Electromagnetic (EM) waves have been widely used in geophysical surveys and underground probing for material characterization, interface detection, and structure identification, based on the capability of EM waves traveling inside dielectric materials (or dielectrics). Such a capability strongly depends on material's EM properties; complex electric permittivity ( $\epsilon^* = \epsilon' - j\epsilon''$ ) and complex magnetic permeability ( $\mu^* = \mu' - j\mu''$ ). The real part of these properties represents the level of energy storage and the imaginary part the level of energy dissipation. For subsurface sensing using EM waves, the real part ( $\epsilon'$  and  $\mu'$ ) is the source for providing dielectric contrast for reflection amplification, while the imaginary part ( $\epsilon''$  and  $\mu''$ ) is responsible for signal attenuation. The fundamental concept of using EM waves for subsurface sensing is to utilize the EM waves reflected from a subsurface target (or anomalies or interfaces) at different frequencies and different incident angles to infer the characteristics of the target. Resolution of EM wave methods is physically governed by wavelength (or frequency) and can be numerically improved by imaging techniques, such as synthetic aperture radar (SAR) imaging.

SAR images of dielectric targets are sensitive to the i) size, ii) geometry, iii) material's EM properties, iv) surface texture/roughness, and v) range. Image resolution is generally affected by the frequency and bandwidth of radar signals, as well as the size of synthetic (artificial) aperture. In practice, higher order coupling effects (e.g., size with geometry) on real structures usually complicate image interpretation for condition assessment, suggesting the need for better understanding of SAR images.

The objective of this paper is to introduce two techniques for the global and local techniques for processing and interpreting SAR images for subsurface sensing of multi-layered civil engineering structural systems, using FRP (fiber reinforced polymer)-concrete specimens as an example. A global technique based on mathematical morphology is introduced for quantifying SAR images for detecting subsurface delamination in glass FRP (GFRP)-concrete systems. The second technique is a method analyzing the local feature of SAR images by

---

Further author information: (Send correspondence to T. Yu)  
E-mail: tzuyang-yu@UML.EDU, Telephone: 1 978-934-2288

utilizing the spatial distribution (Gaussian curvature  $K$ , area ratio  $R$ , and amplitude ratio  $I$ ) of amplitudes in SAR images for detecting subsurface delamination in carbon FRP (CFRP)-concrete systems.

In this paper, principle of SAR imaging is briefly introduced. Description of laboratory specimens used both techniques is then provided. Procedure of the global, mathematical morphology technique is explained. Concept of the local (or  $K - R - I$ ) technique is described. Performance these two techniques is demonstrated using laboratory FRP-concrete specimens.

## 2. APPROACH

### 2.1 SAR Imaging

In SAR imaging of radar signals, only reflected/returned radar signals are utilized and processed by SAR and backprojection algorithms.<sup>1,2</sup> Key steps in SAR imaging are briefly described in the following. In the EM scattering of a general target, its coherent SAR point response collected by radar sensor can be defined by

$$S(x, y \sin \theta_i) = \text{sinc} \left( \frac{\pi y \sin \theta_i}{\rho_r} \right) \text{sinc} \left( \frac{\pi x}{\rho_{xr}} \right) \quad (1)$$

where  $(x, y, z) =$  coordinates on the plane of radar inspection,  $\theta_i =$  incident angle with respect to the  $z$  axis,  $\rho_r =$  range resolution of the radar, and  $\rho_{xr} =$  cross-range resolution of the radar.  $\text{sinc}(x) = \frac{\sin(x)}{x}$  is the sinc function. Define the distance between a single scatterer and the radar to be  $\bar{r}_{s,j}$  where  $s$  denotes the scatterer and  $j$  the radar. Figure 1 illustrates the definition of inspection angle  $\theta_i$  on the image plane. The coherent SAR

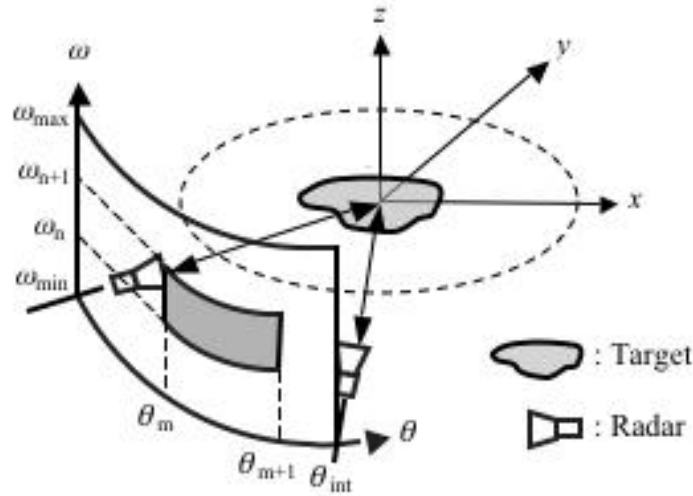


Figure 1. Definition of inspection angle on the image plane (modified from<sup>2</sup>)

point response can also be represented by

$$S(\bar{r}_{s,j}) = \text{sinc} \left( \frac{\pi r_{s,j}}{\rho} \right) \quad (2)$$

where  $r_{s,j} = |\bar{r}_{s,j}|$  and  $\rho = \sqrt{\rho_r^2 + \rho_{xr}^2}$ . The time-dependent  $S(\bar{r}_{s,j})$  can be written by

$$S(\bar{r}_{s,j}, t) = \frac{1}{r_{s,j}^2} \int_{\omega_c - \pi B}^{\omega_c + \pi B} d\omega \cdot \exp[i\omega t] \quad (3)$$

where  $\omega_c$  = the carrier frequency,  $B$  = the frequency bandwidth,  $i = \sqrt{-1}$  = the imaginary number, and  $t$  = the time variable. The range compression on  $S(\bar{r}_{s,j}, t)$  is carried out by shifting  $t$  to  $\hat{t} = t - \frac{r_{s,j}}{c}$  ( $c$  is the speed of radar signals). The integral in Eq.(3) leads to

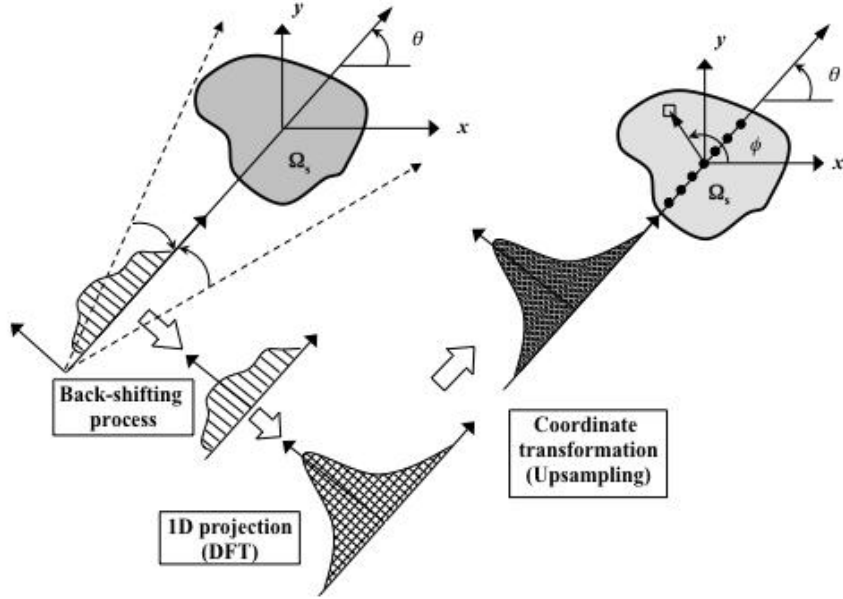


Figure 2. Concept of subsurface radar imaging (modified from<sup>2</sup>)

$$S(\bar{r}_{s,j}, \hat{t}) = \frac{B}{r_{s,j}^2} \exp[i\omega_c \hat{t}] \cdot \text{sinc}(B\hat{t}) \quad (4)$$

After performing range-compression on focused radar signals, we integrate all range-compressed focused radar signals to obtain  $D(\xi, \hat{t})$ , where  $\xi$  is the position of the radar traveling on its synthetic aperture. The backprojection processing is performed by

$$B_{BP}(\xi, t) = C_{BP} \cdot \frac{\partial D(\xi, \hat{t})}{\partial t} \quad (5)$$

where  $C_{BP}$  = the backprojection coefficient defined in order to yield an ideal bandpass transfer function. Finally, the backprojected SAR image is obtained by

$$I(\bar{r}, \phi) = \int_0^{r_s \theta_{\text{int}}} d\xi \cdot B_{BP}(\xi, \hat{t}) = I(r, r_x) \quad (6)$$

where  $(\bar{r}, \phi)$  = polar coordinates on SAR images, and  $(r, r_x)$  = range-cross-range (rectangular) coordinates on SAR images. Conversion between  $(\bar{r}, \phi)$  and  $(r, r_x)$  can be carried out by the conversion between polar and Cartesian coordinate systems. From this formulation, it is evident that the resolution of SAR images can be improved by bandwidth ( $B$ ), frequency ( $\omega_c$ ), and synthetic aperture ( $\theta_{\text{int}}$ ). Time-space projection is performed by using the velocity of radar signals. SAR imaging and backprojection algorithms have been demonstrated as a promising technique in the subsurface sensing of construction materials such as FRP and Portland cement concrete in civil engineering. Their use on the detection of subsurface debonding in multi-layer composite-concrete systems has also been reported.<sup>3</sup> Further information on the remote sensing theories can be found in related literature.<sup>4-6</sup>

## 2.2 Global Technique – Mathematical Morphology

The first technique introduced is the combination of mathematical morphology and Euler's number. Mathematical morphology enables researchers to extract the global features of SAR images. Quantification of feature extracted SAR images is achieved by using Euler's number. Additional information about mathematical morphology can be found in the literature.<sup>?,?,?</sup> In this paper, a three-step mathematical morphology processing is used.

1. Thresholding – To extract the characteristic shape of a SAR image, the image is first transformed into a binary image based on a threshold value  $n_{thv}$ . This threshold value defines the minimum SAR amplitude that will be subjected to morphological processing in the following steps. Optimal threshold value is empirically determined by the most drastic change of Euler's number  $n_E$  of each SAR image. A binary, thresholded SAR image  $I(r, r_x|n_{thv})$  can be obtained.
2. Erosion – Once the binary SAR image is obtained, an erosion operator defined by Eq.(7) is applied to the image.

$$\epsilon_K(I) = \{r|K_r \subseteq I(r, r_x|n_{thv})\} \quad (7)$$

where  $\epsilon_K$  = erosion operator with an erosion structure  $K$ , and  $K_r$  = eroded set operating at position  $r$ .

3. Dilation – After the binary SAR image is processed by the erosion operator, an dilation operation defined by Eq.(8) is subsequently applied to the image.

$$\delta_V(I) = \{r|V_r \cap I(r, r_x|n_{thv}) \neq \emptyset\} \quad (8)$$

where  $\delta_V$  = dilation operator with an erosion structure  $V$ , and  $V_r$  = eroded set operating at position  $r$ .

After the morphological processing, the original SAR image becomes

$$\hat{I}(r, r_x|n_{thv}) = \delta_V(\epsilon_K(I(r, r_x|n_{thv}))) \quad (9)$$

This binary, feature-extracted SAR image is ready to be quantified. Euler's number  $n_E$  is used in characterizing the feature of  $\hat{I}(r, r_x|n_{thv})$ .

$$n_E(\hat{I}(r, r_x|n_{thv})) = n_o(\hat{I}) - n_h(\hat{I}) \quad (10)$$

where  $n_o$  = number of objects in  $\hat{I}$ , and  $n_h$  = number of holes inside the objects in  $hatI$ .

## 2.3 Local Technique – $K - R - I$ Transform

Another approach focusing on quantifying local features of SAR images is the  $K - R - I$  transform.<sup>7</sup> In the three-dimensional representation of SAR images  $I(r, r_x)$ , the following parameters are calculated from each image.

$$K_{avg}(C_i(I_i)) = \frac{1}{n} \sum_{i=1}^n K_i(r, r_x) \quad (11)$$

$$R(C_i) = \frac{A(C_i)}{A_{\max}} \quad (12)$$

$$I(C_i) = \frac{I_i}{I_{\max}} \quad (13)$$

where  $K_{avg}(C_i(I))$  = average Gaussian curvature at contour  $C_i$ ,  $C_i$  = contour of enveloped area at a given SAR amplitude  $I_i$ ,  $n$  = number of SAR amplitudes,  $R(C_i)$  = area ratio of  $C_i$ , and  $I(C_i)$  = SAR amplitude ratio of  $C_i$ .

### 3. EXPERIMENTATION

#### 3.1 Description of Specimens

Laboratory FRP-concrete cylinders with artificial defects were designed for validating SAR image processing techniques. Glass FRP-wrapped concrete and carbon FRP-wrapped concrete cylinders were manufactured, as shown in Figs. 3 and 3. An artificial defect was introduced at the interface between FRP wrap and the concrete core in each FRP-concrete cylinder.

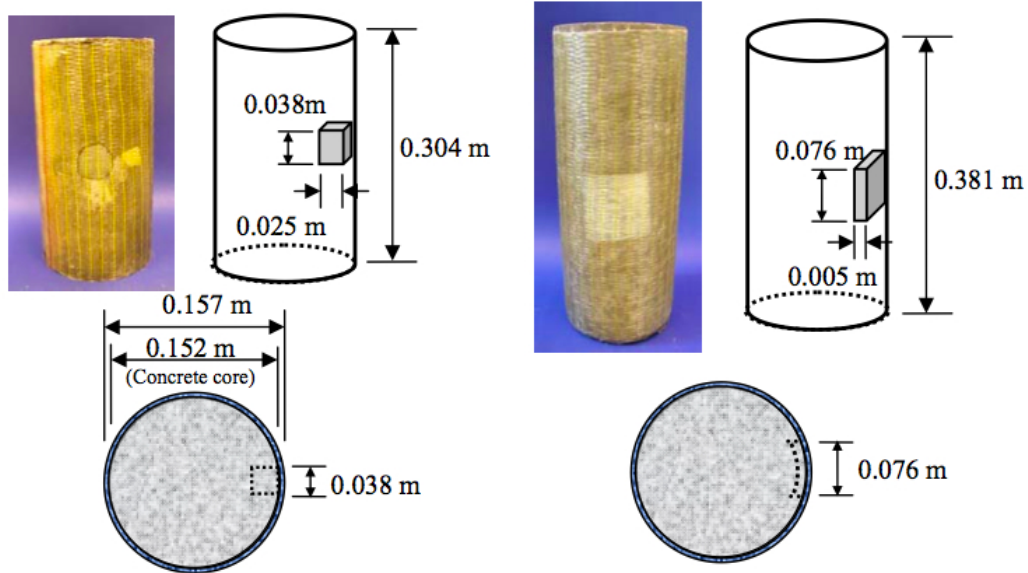


Figure 3. Two artificially-damaged GFRP-concrete cylinders (modified from<sup>2</sup>)

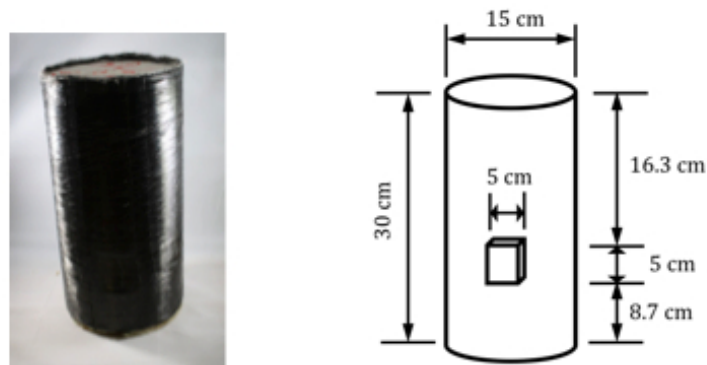


Figure 4. One artificially-damaged CFRP-concrete cylinder (modified from<sup>7</sup>)

#### 3.2 Physical Radar Measurement

SAR imaging was conducted inside an anechoic chamber in the Department of Civil and Environmental Engineering at the University of Massachusetts Lowell. This radar facility is capable of conducting distant radar measurements in the frequency range of 1 GHz to 18 GHz. Fig. 5 shows the imaging radar facility used in this paper.



Figure 5. Custom-built anechoic chamber, 1 GHz-18 GHz; (left) exterior of the chamber, (right) interior of the chamber with a reinforced concrete beam specimen (CEE, UML)

#### 4. IMAGING RESULTS

Figs. 6 and 7 show the imaging result of a GFRP-concrete cylinder inspected from its intact and damaged sides. HH and VV polarized radar signals were used. The SAR images processed by mathematical morphology are

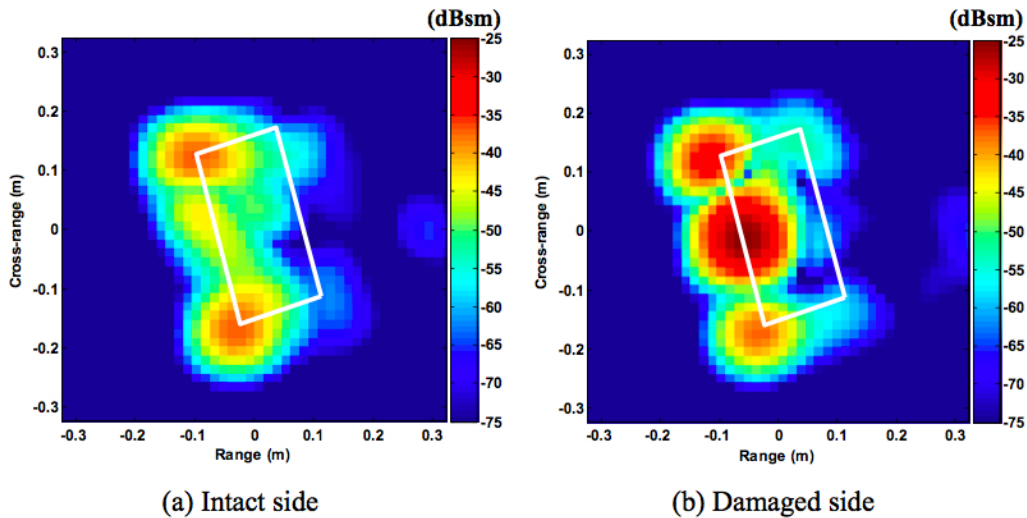


Figure 6. SAR images of GFRP-concrete cylinders; intact and damaged sides

shown in Fig. 8. Computed Euler's numbers at different incident angles are shown in Fig. 9, after subjected to a three-point low pass filter. SAR imaging result of both the intact and damaged sides of the CFRP-concrete cylinder is shown in Figs. 10 and 11, along with their  $K - R - I$  curves.  $K - R - I$  transform was applied to SAR images collected at different angles and compared with the signal-to-noise ratio (SNR) at the location in SAR images where the defect was embedded. Coefficient of correlation was also calculated to quantified the difference between the  $K - R - I$  curves of the intact side and the ones of the damaged side. Result is shown in Fig. 12.

From these results, findings are summarized in the following.

- Mathematical morphology processing provides an opportunity to extract features of SAR images to enable image quantification using Euler's number. The use of thresholding is key in determining the representative Euler's number.

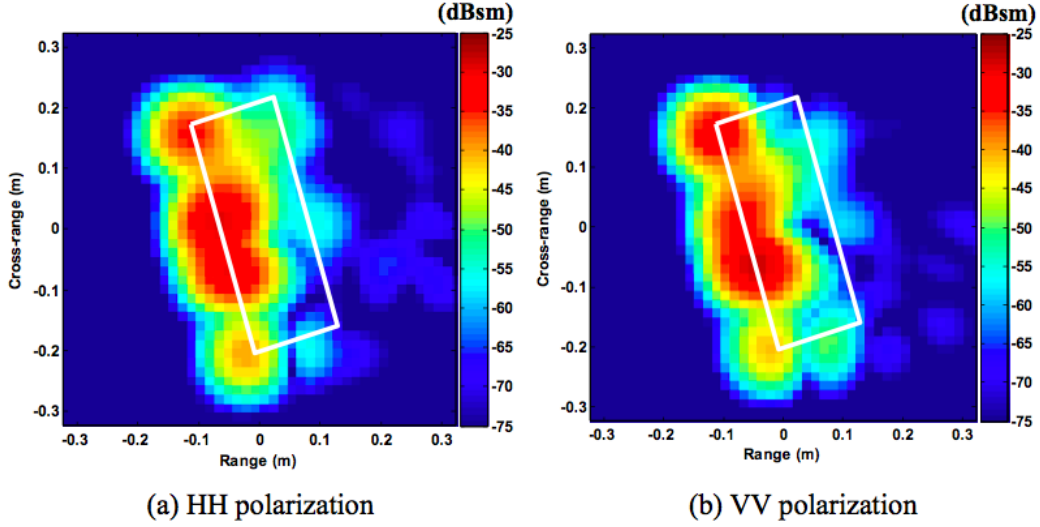


Figure 7. SAR images of GFRP-concrete cylinders; damaged side

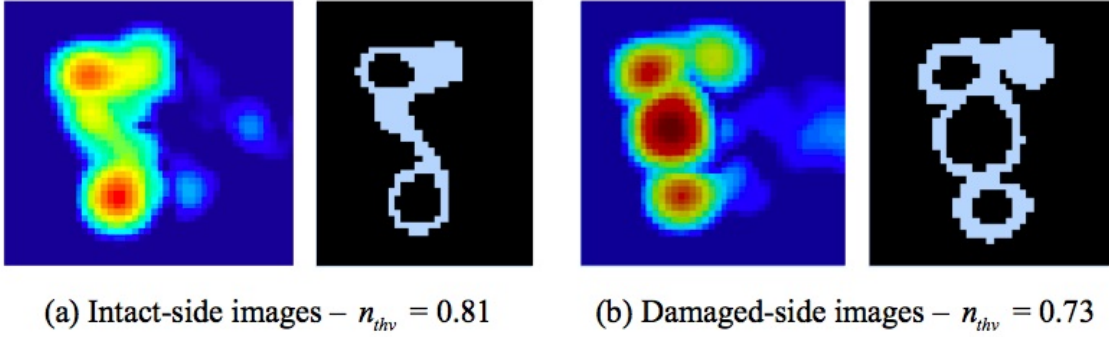


Figure 8. Processed SAR images using mathematical morphology

- While Euler's number shows promising result in differentiating SAR images of intact and damaged structures, it has limitations on i) selecting an appropriate threshold value for Euler's number and ii) differentiating intact and damaged curves of Euler's number at certain incident angles ( $0^\circ$   $10^\circ$  in Fig. 9).
- The  $K - R - I$  transform represents a different approach to quantify SAR images. From Fig. 12, it can be deduced that damaged structures should exhibit  $K - R - I$  curves different from the ones of intact structures, suggesting a low coefficient of correlation.
- In Fig. 12, all the coefficients of correlation between intact and damaged SAR image curves are less than unity. This result indicates that the  $K - R - I$  transform improves the constraint and difficulty of mathematical morphology on quantifying SAR images.

## 5. CONCLUSION

Understanding SAR images can lead us to the better use of EM waves for the surface and subsurface sensing of construction materials and structures such as Portland cement concrete. Global and local techniques represent different perspectives to characterize SAR images. From the results presented in this paper, the  $K - R - I$  transform outperforms mathematical morphology on the detection of subsurface defect in a multi-layered system like FRP-concrete cylinders.

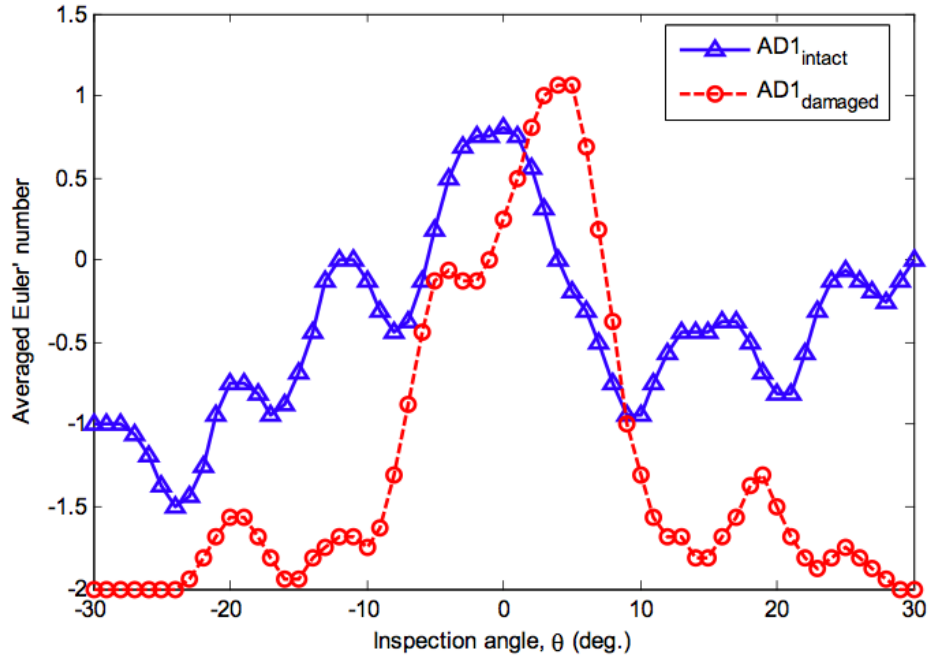


Figure 9. Euler's number of SAR images at different incident angles; GFRP-concrete cylinder

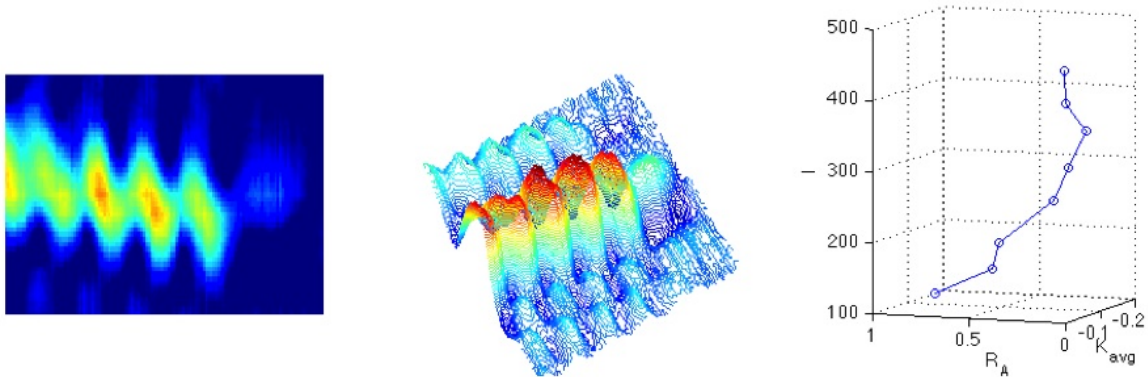


Figure 10. SAR image of a CFRP-concrete cylinder; intact side

## 6. ACKNOWLEDGMENTS

This work was partially supported by the U.S. Department of Transportation (DOT) Research and Innovative Technology Administration (RITA) Commercial Remote Sensing and Technology (CRS&SI) Program through Grant OASRTRS-14-H-UML.

## 7. DISCLAIMER

The views, opinions, findings and conclusions reflected in this presentation are the responsibility of the authors only and do not represent the official policy or position of the USDOT/RITA, or any State or other entity.

## REFERENCES

- [1] Yegulalp, A. F., "Fast backprojection algorithm for synthetic aperture radar," in *[Proc. of IEEE Radar Conf.]*, 60–5, IEEE (1999).
- [2] Yu, T., "A distant damage assessment method for multi-layer composite systems using electromagnetic waves," *J. Eng. Mech.* **137**(8), 547–560 (2011).

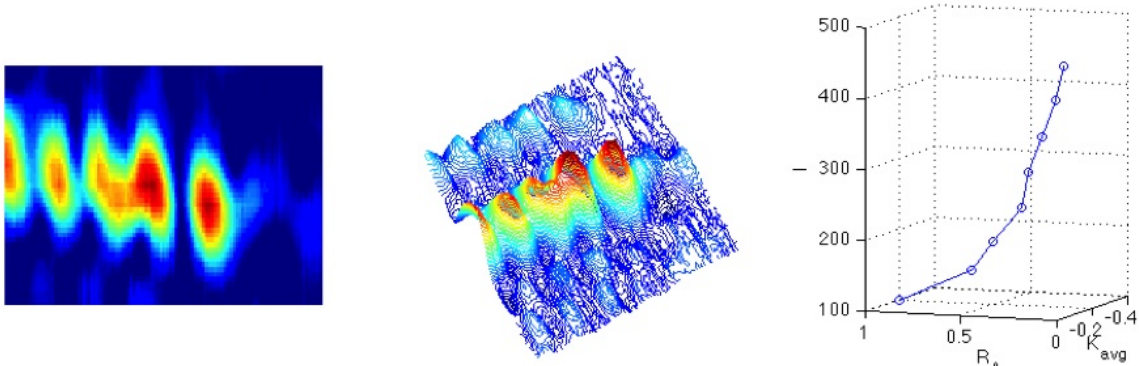


Figure 11. SAR image of a CFRP-concrete cylinder; damaged side

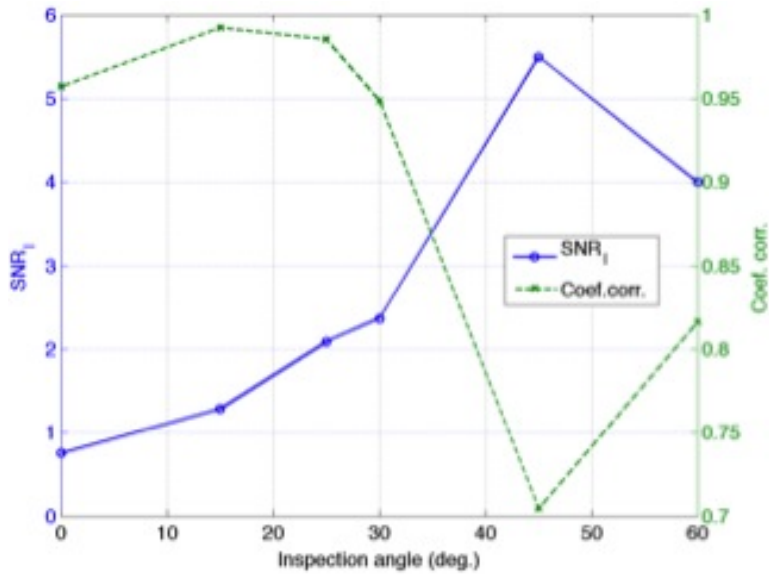


Figure 12. SAR image of a CFRP-concrete cylinder; damaged side

- [3] Yu, T.-Y., "Determining the optimal parameters in a distant radar nde technique for debonding detection of gfrp-concrete systems," in [*Proc. SPIE*], **7294** (2009).
- [4] Soumekh, M., [*Synthetic aperture radar signal processing with MATLAB algorithms*], Wiley, New York, NY (1999).
- [5] Kong, J. A., [*Electromagnetic Wave Theory*], EMW Publishing, Cambridge, MA (2000).
- [6] Tsang, L., Kong, J. A., and Ding, K.-H., [*Scattering of Electromagnetic Waves – Theories and Applications*], John Wiley & Sons, New York (2000).
- [7] Yu, T., "Quantitative assessment of cfrp-concrete cylinders using synthetic aperture radar images," *RNDE April*, 1–18 (2016).